

# Double PM-Rotor, Toothed, Toroidal-Winding Wind Generator: A Comparison With Conventional Winding Direct-Drive PM Wind Generators Over a Wide Power Range

Johannes H. J. Potgieter, *Member, IEEE*, and Maarten J. Kamper, *Senior Member, IEEE*

**Abstract**—The double rotor, toothed, toroidal-winding permanent-magnet (PM) machine is not a well known concept and has received very limited attention in literature. In this study, the concept is proposed for use as a direct-drive wind generator. Due to the varying design requirements of wind generators over the different power ranges, the PM generator is optimized over the entire installed wind power range. For each power level, the optimum design is compared with optimum nonoverlap-winding and conventional overlap-winding PM machine designs. This also gives a much broader indication on the scaling of different wind generator technologies. Although the electromagnetic design, by means of finite-element analysis, of the generator is the main focus of the paper, some of the implementation issues are also discussed. An existing 15-kW double rotor PM wind generator is modified to include a toroidal-winding, which is used as a case study. Both simulated results and practical measurements in the laboratory for the 15-kW case study toroidal-winding PM generator are presented in this paper.

**Index Terms**—Design optimization, finite-element (FE) analysis, generators, permanent-magnet (PM) machines, toroidal magnetic fields, wind energy generation, wind energy integration.

## NOMENCLATURE

$D_i$	Generator inner diameter (mm).
$D_o$	Maximum outer diameter (mm).
$f_s$	Peak electrical frequency (Hz).
$\mathbf{G}, g_{1-n}$	Design constraints.
$h_c$	Stator conductor height (mm).
$h_m$	Permanent-magnet (PM) height (mm).
$h_{ry}$	Rotor yoke height (mm).
$h_{sy}$	Stator yoke height (mm).
$I_s$	Generator rms current (A).

$J_s$	Stator rated rms current density (A/mm <sup>2</sup> ).
$l$	Axial length of generator (mm).
$M_{Cu}$	Conductor mass (kg).
$M_{Fe}$	Electrical steel mass (kg).
$M_{PM}$	PM mass (kg).
$M_{Tot}$	Total active mass (kg).
$n_s$	Rated turbine speed (r/min).
$p$	Number of rotor poles.
$P_{cu}$	Stator winding dc conductor losses (W).
$P_{cue}$	Stator winding ac conductor losses (W).
$P_{ecr}$	PM-rotor core and PM eddy-current losses (W).
$P_{ecs}$	Stator core losses (W).
$P_{NL}$	No-load frequency dependent losses (W).
$P_{wf}$	Wind and friction losses (W).
$R_s$	Per-phase stator winding resistance ( $\Omega$ ).
$T_b$	Maximum breakdown torque (p.u).
$T_r$	Average-rated generator torque (Nm).
$v_w$	Wind speed (m/s).
$V_{act}$	Generator active stack volume (m <sup>3</sup> ).
$X_s$	Synchronous reactance ( $\Omega$ ).
$\mathbf{X}, x_{1-n}$	Dimensional input parameters.
$\mathbf{Y}, y_{1-n}$	Design objectives.
$\alpha_s$	Electrical current angle measured from the $q$ -axis ( $^\circ$ ).
$\Delta\tau_L$	Rated load torque ripple (%).
$\Delta\tau_{NL}$	No-load cogging torque (%).
$\eta_s$	PM generator efficiency (%).
$\sigma_m$	Ratio of PM angle to pole angle.
$\sigma_w$	Ratio of slot width to average slot pitch.

## I. INTRODUCTION

ALTHOUGH most installed wind turbine systems make use of the geared doubly fed induction generator and partially rated converter topology, direct-drive wind generators are utilized in several new installations in order to decrease the number of components in the drive train. This eliminates the maintenance issues associated with gearboxes, which should, thus, in turn reduce the operation and maintenance (O&M) costs of the wind turbine system. Utility-scale direct-drive wind turbine systems make use of both wound synchronous generator (WSG) and PM synchronous generator (PMSG) topologies. Small-scale wind generators mostly utilize directly turbine-mounted PMSGs. However, due to the current

Manuscript received September 16, 2015; revised November 20, 2015 and February 2, 2016; accepted February 4, 2016. Date of publication March 1, 2016; date of current version July 15, 2016. Paper 2015-EMC-0735.R2, presented at the 2014 International Conference on Electrical Machines, Berlin, Germany, September 2–5, and approved for publication in the IEEE TRANSACTIONS ON INDUSTRY APPLICATIONS by the Electric Machines Committee of the IEEE Industry Applications Society. This work was supported by the National Research Foundation (NRF) of South Africa.

J. H. J. Potgieter is with the Department of Engineering Science, University of Oxford, Oxford, OX1 2JD, U.K. (e-mail: johannes.potgieter@eng.ox.ac.uk).

M. J. Kamper is with the Department of Electrical and Electronic Engineering, Stellenbosch University, Stellenbosch 7602, South Africa (e-mail: kamper@sun.ac.za).

Color versions of one or more of the figures in this paper are available online at <http://ieeexplore.ieee.org>.

Digital Object Identifier 10.1109/TIA.2016.2536580

high price of PM material, PMSGs are losing their attractiveness, due to these types of systems currently being the most expensive [1]. Due to the high costs associated with direct-drive utility-scale PM wind generators, many are also considering high-speed and medium-speed PM wind generators, as in [2]. Some manufacturers are also again installing the conventional squirrel cage induction generator and multistage gearbox due to the low initial capital cost of this system, with the generator connected to the grid via a full-rated converter, in order to comply with the relevant grid code specifications. For offshore systems, though, direct-drive wind generators are being favored in many cases due to their lower O&M requirements.

From the discussion above, it is, thus, evident that in order for direct-drive PM wind generators to remain competitive, the cost of these generators needs to be reduced. Several works on the design and comparison of direct-drive PM generators with regard to other drive-train topologies are available in literature, as in [3]–[11]. The major issues identified in the design and implementation of direct-drive PM wind generators are the high cost and volatility of PM prices, the high active mass, and also high structural mass at higher power levels, as well as the large size which makes assembly, installation, and transport difficult. It is, thus, essential that the mass and PM content of these generators be made as low as possible.

Dual rotor PM machine topologies have been proposed for wind generators before as in [7] and [12]. However, in the case of conventional overlap-winding machines, the relatively large end-windings make it difficult to assemble the machine, with the eventual configuration not at the optimum machine dimensions. Many dual rotor PM machine topologies also have the disadvantage of a larger effective airgap. In this case, it might be better to go for the toothed toroidal type of topology such as in [13] and [14] and more recently in [15] and [16] as proposed for wind generators.

In this paper, the toothed toroidal-winding wind generator is evaluated with respect to other direct-drive wind generator topologies such as conventional overlap-winding and nonoverlap-winding PM wind generator configurations. Although this generator type has been proposed before for direct-drive wind generators as in [15] and [16], there is a lack of a clear indication in literature as to the applicability and advantages of this generator type with regards to other topologies currently in use. To obtain a better indication regarding the applicability of the toroidal-winding wind generator and to obtain a better idea with regards to the scaling of conventional wind generator technologies in general, optimization results are presented over the 1.0 kW to 7.5 MW wind turbine power range. This work follows a similar approach as in [17], where a new concept wind generator is compared over the power range from 30 kW to 3 MW. Further information on the scaling of direct-drive wind generators can also be found in [18]. It should be noted that the focus of this paper is predominately on the electromagnetic design and does not include any detailed thermal or structural analysis.

Wind turbine power ranges are broadly categorized as small scale, medium scale, and utility scale. Although there are many definitions for the power ranges of small-scale wind turbines, small-scale systems are mostly considered as anything below

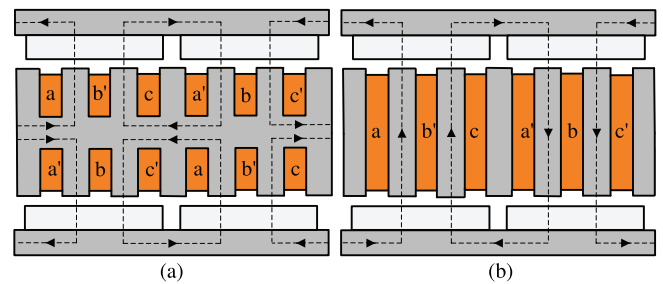


Fig. 1. Flux paths for (a) new concept toothed toroidal-winding and (b) conventional type, double rotor PM machine topologies.

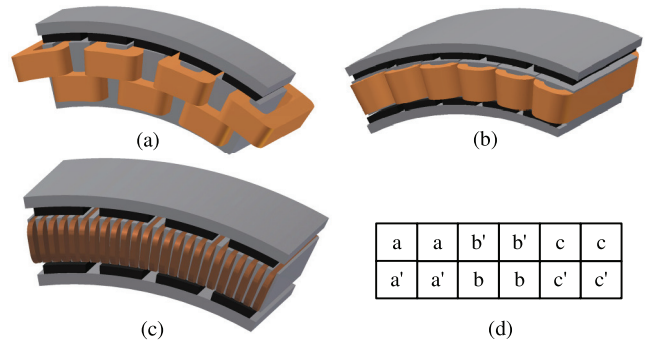


Fig. 2. (a) Single and (b) double rotor nonoverlap double layer winding and (c) double rotor toothed toroidal-winding PM wind generator topologies. (d) Phase layout diagram for the toroidal-winding over one pole [16].

100 kW, with around more or less 1 kW and less considered as micro or pico wind power generation. The range between about 100 and 500 kW and maybe even up to 1 MW is considered as medium-scale wind power generation, and above 1 MW is considered as utility scale. Small- and medium-scale wind generator systems have been around for a long time and significant growth is currently observed and predicted in this wind power segment, especially for rural and off-grid applications. However, very little research exists on small-scale systems as compared to utility-scale wind turbines, which justify the inclusion of this wind power range in this study.

Finite-element (FE) simulated results and practical laboratory measurements are given for a case study toroidal-winding wind generator. This generator is constructed by modifying an existing 15-kW double rotor direct-drive PM wind generator, which is the same prototype machine as evaluated in [12].

## II. TOOTHED TOROIDAL-WINDING GENERATOR CONCEPT

Normally, toroidally wound coils are wound around a steel cylinder with the stator being toothless. This allows for easier manufacturing, but the drawback is a large airgap that requires more PM material. In this study, a slotted stator configuration is used with slots on both the inner and the outer diameters of the stator, with a common stator yoke as shown in Fig. 1(a). The machine is assembled in a way that two opposing magnet polarities face one another. The flux from the inner magnet links the inner stator conductor, and the flux from the outer magnet links the outer stator conductor. Fig. 1(b) shows a conventional double rotor topology, where the flux of the outer and inner PMs link through the stator section of the machine. Fig. 2(a) shows

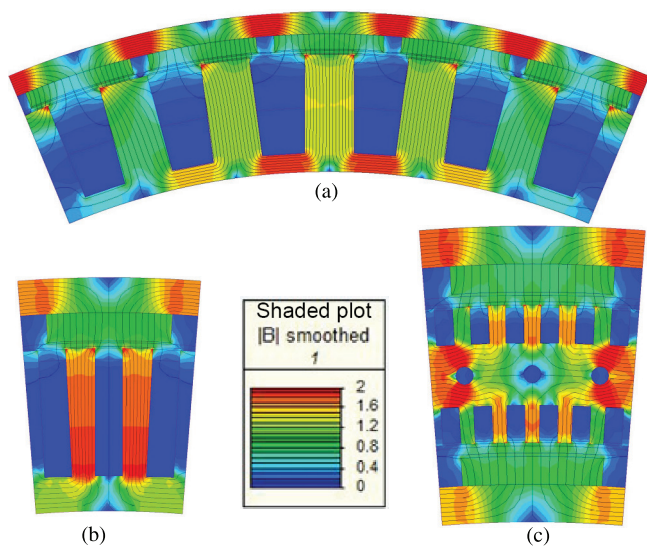


Fig. 3. FE field plots for conventional (a) nonoverlap double layer and (b) three-phase overlap-winding, and (c) double rotor toothed toroidal-winding PM wind generator topologies [16].

an example of a more conventional-type single rotor, double layer, nonoverlap-winding PM machine, of which the design and evaluation is more thoroughly covered in [16]. Fig. 2(b) shows a double rotor variant of this winding type as is evaluated in [12]. An example of the toroidal-winding topology considered in this study is shown in Fig. 2(c), with Fig. 2(d) showing the phase layout over one pole of this winding type when utilizing six slots per pole. Fig. 3(a) and (b) shows the field plots for the single rotor conventional nonoverlap- and overlap-winding configurations and Fig. 3(c) for the toothed toroidal-winding generator at the 15-kW power level. It is clear that there is saturation in the teeth and yokes of the machines, and this is taken into account in the nonlinear FE solution that is used by the optimization algorithm in the design optimization of the generators.

Depending on the number of poles and stator yoke height, a significant advantage of the double rotor toroidal-winding PM generator is the fact that none of the coils are overlapping, which means that the size of the end-windings is significantly reduced as compared to conventional overlap-windings. The copper losses and mass are, thus, reduced accordingly. Furthermore, stator segmentation, which is especially a consideration for large wind generators, should not be a problem in this type of winding due to nonoverlapping coils. Due to this generator utilizing a three-phase winding layout, it should also have a much better torque performance when compared to nonoverlap-winding topologies. Currently, it is difficult to comment on the manufacturability of the double rotor toroidal-winding generator, as this type of configuration has not yet been used for wind generators. Although this machine has been practically evaluated in literature, such as in [13] and [14], and good results were obtained, the reason why it has not received widespread adoption in industry might be that it has only been implemented for low pole number radial flux machines. At low pole numbers, the use of this type of configuration is questionable due to the large common yoke that would be required,

TABLE I  
DESIGN SPECIFICATIONS AT DIFFERENT WIND POWER  
LEVELS CONSIDERED

	$T_r$ (kNm)	$T_b$ (pu)	$\eta_s$ (%)	$n_s$ (r/min)	$p$	$f_s$ (Hz)	$D_o$ (m)
1.00 kW	0.012	2.0	92	800	10	67	0.3
3.00 kW	0.13	2.0	92	300	20	50	0.510
15.0 kW	1.0	2.0	94	150	40	50	0.655
60.0 kW	7.35	1.1–1.5	94	78	60	39	1.2
300 kW	67	1.1–1.5	95	50	70	29	2.5
1.00 MW	330	1.1–1.5	95	29	160	39	3.5
3.00 MW	1910	1.1–1.5	95	15	160	20	5.0
7.50 MW	6120	1.1–1.5	95	12	160	16	12

which increases the end-winding length and reduces the airgap diameter of the bottom PM rotor. Furthermore, if the common stator yoke saturates, unwanted coupling effects might occur between the outer and the inner PM rotors.

### III. DESIGN SPECIFICATIONS AND METHODOLOGY

In previous studies of the toroidal-winding PM wind generator, such as in [16], a comparison between different winding configurations is only done at the 15-kW power level. As far as possible, in this study, reference designs for direct-drive generators from literature are used for comparison over the entire installed wind turbine power range.

#### A. Design Specifications

The design optimization is done for the power levels of 1 kW [19], 3 kW [20], 15 kW [16] and [21], 60 kW [17], 300 kW [22], 1 MW [17], 3 MW [3], and 7.5 MW [23] and [24]. Table I gives the design constraints for different wind generator power levels considered.

For smaller generators, more or less microscale, a minimum efficiency of 92%, as is also specified in [20], is selected. For the small-scale power range up to 60 kW, an efficiency of  $\eta_s > 94\%$  is specified, which is the same as in [16]. For all the generators larger than 60 kW, it is specified that  $\eta_s > 95\%$ , which is mostly considered as a feasible value in literature for larger generators. The rated rotor speed ( $n_s$ ), rated torque requirement, and maximum allowable outer diameter ( $D_o$ ) are found from the relevant reviewed literature works. The generator outer diameter is mostly determined by the turbine characteristics for smaller systems, because if the outer diameter becomes too large, the generator structure interferes with the aerodynamic properties of the wind turbine. For larger systems, factors such as manufacturing constraints, transportation, installation, and other logistical factors largely influence the outer diameter. Fig. 4 shows the maximum allowable outer diameter versus wind generator power rating. It is clear from Fig. 4 that as the generator power increases, the increase in  $D_o$  is increasingly more constrained. The 7.5-MW wind generator from [23] is included for the sake of interest. This generator is different from the other direct-drive topologies, as it has a wound rotor and the outer diameter of 12 m is considered extremely large for direct-drive wind generators.

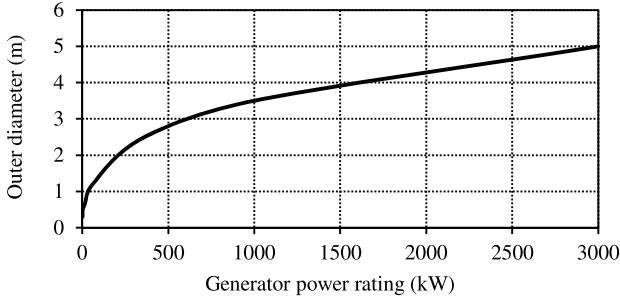


Fig. 4. Maximum PM generator outer diameter versus turbine power rating.

Due to the higher rotational speed, the number of poles ( $p$ ) selected for the smaller systems cannot be too high, as the electrical frequency ( $f_s$ ) will be too high, which will significantly increase the no-load losses,  $P_{NL}$  [defined in (3)], of the generator. Depending on the speed range of the generator, frequency-dependant losses could largely influence the partial load efficiency. For the utility-scale generators,  $p$  is kept constant to ease implementation of the models. Normally, an optimum value for  $p$  considering rotor mass and  $P_{NL}$  would be selected.

Other aspects to consider include ease of manufacturing and stator segmentation, especially for larger generators. Furthermore, important in the design of PM generators is the load torque ripple and especially the no-load cogging torque as explained in [21]. In [25], it is specified that the cogging torque of direct-drive PM wind generators should be at least in the range 1.5%–2%. In some cases, it is specified as low as 0.5%. However, for comparison purposes as also done in [16], a no-load cogging torque value of  $\Delta\tau_{NL} < 2\%$  and a load torque ripple value of  $\Delta\tau_L < 4\%$  are chosen. As no thermal analysis is included in this optimization, a maximum rms current density of  $J_s < 4 \text{ A/mm}^2$  is assumed, which is deemed acceptable for natural convection air cooling by [26]. This is true for the smaller generators; however, for utility-scale generators, better cooling methods are utilized, which means that higher current densities can be tolerated. In [27], liquid cooling for large direct-drive wind turbines are discussed and current densities of  $J_s > 6 \text{ A/mm}^2$  are reported.

Most of the smaller wind turbine systems make use of passive yawing, fixed blade pitch, passive furling for high wind speed protection, and electromagnetic braking. For electromagnetic braking, it is found from previous practical iterations that the maximum breakdown torque ( $T_b$ ) of the smaller generators should be specified as at least  $T_b > 2 \text{ p.u.}$  It is also mentioned in [28] that generators utilizing stall speed control have higher torque ratings. For systems larger than 50 kW, which utilize variable pitch and other forms of braking, the maximum torque of the generator is usually in the range  $1.1 < T_b < 1.5 \text{ p.u.}$  The average-rated torque ( $T_r$ ) at rated wind speed and turbine speed is used as the base value in all cases.

### B. Optimization Methodology

To ease implementation in the design optimization of different machine structures at different power levels, the winding

layouts are kept as similar as possible in all cases. For the nonoverlap-winding, the high winding factor 10/12 pole slot combination, as also used in [21], is selected with a double layer winding layout. For the conventional three-phase overlap-winding, three slots per pole is utilized throughout the design optimization. Up to a maximum of six slots per pole is utilized for the toroidal-winding generators.

All of the wind generators considered in this study are optimized for minimum active mass ( $M_{Tot}$ ) and minimum PM mass ( $M_{PM}$ ), subject to certain design constraints, as explained later in this paper. The design optimization is done by means of the *Visual Doc* optimization suite [29], which is coupled with static FE analysis to reduce simulation times. From different optimization algorithms available in *Visual Doc*, the gradient-based, modified method of feasible directions (MMFDs) is selected. This method is shown to consistently give the best results in the shortest amount of time for this particular study. More information on the optimization algorithms best suited for electrical machine design can be found in [30]. A typical static FE function evaluation takes about 15 s, and depending on the number of function evaluations, a successfully converged optimization run takes about 2 h. For each optimum topology, about three to four optimization runs are required to obtain the optimum design. After the static FE optimization, a transient FE verification is done and slight modifications is made to the optimized machine in order to ensure that it complies with the relevant design constraints. The machine design optimization parameters are indicated by  $\mathbf{[X]}$ , the output performance parameters in the objective function are indicated by  $\mathbf{[Y]}$ , and the design constraints are given by  $\mathbf{[G]}$  with

$$\mathbf{X} = \begin{bmatrix} l \\ h_c \\ h_m \\ h_{ry} \\ h_{sy} \\ \sigma_w \\ \sigma_m \\ P_{cu} \end{bmatrix} \quad \mathbf{G} = \begin{bmatrix} T_r \\ T_b \\ \Delta\tau_{NL} \\ \Delta\tau_L \\ \eta_s \\ J_s \end{bmatrix} \quad \mathbf{Y} = \begin{bmatrix} y_1 \\ y_2 \end{bmatrix} = \begin{bmatrix} M_{Tot} \\ M_{PM} \end{bmatrix} \quad (1)$$

with  $\mathbf{F}[\mathbf{Y}] = \text{objective function} = w_1 y_1 + w_2 y_2$ . The values of the constraints in  $\mathbf{[G]}$  are given in Table I and as explained above. Fig. 5 shows a graphical representation of the optimization workflow in this study. In each case, the current angle measured from the  $q$ -axis ( $\alpha_s$ ) is set to zero for maximum torque per ampere. The conductor loss ( $P_{cu}$ ) is made variable in the design optimization in order to enable the optimization algorithm to specify an operating point with  $I_s^2 = P_{cu}/3R_s$ .

For the toroidal-winding PM machine,  $h_m$ ,  $h_{ry}$ , and  $\sigma_m$  in (1) consists of two components, for the outer and inner PM rotors, respectively. Furthermore, in this case, for the toroidal-winding machine to ease manufacturing,  $h_c$  and  $\sigma_w$  are taken as the same value for the outer and inner slots. The efficiency in (1) is calculated from the total losses with

$$P_{Loss} = P_{cu} + P_{ecs} + P_{ecr} + P_{wf} \quad (2)$$

where  $P_{ecs}$  and  $P_{ecr}$  indicate the stator core losses and the PM-rotor losses, respectively. The wind and friction losses indicated

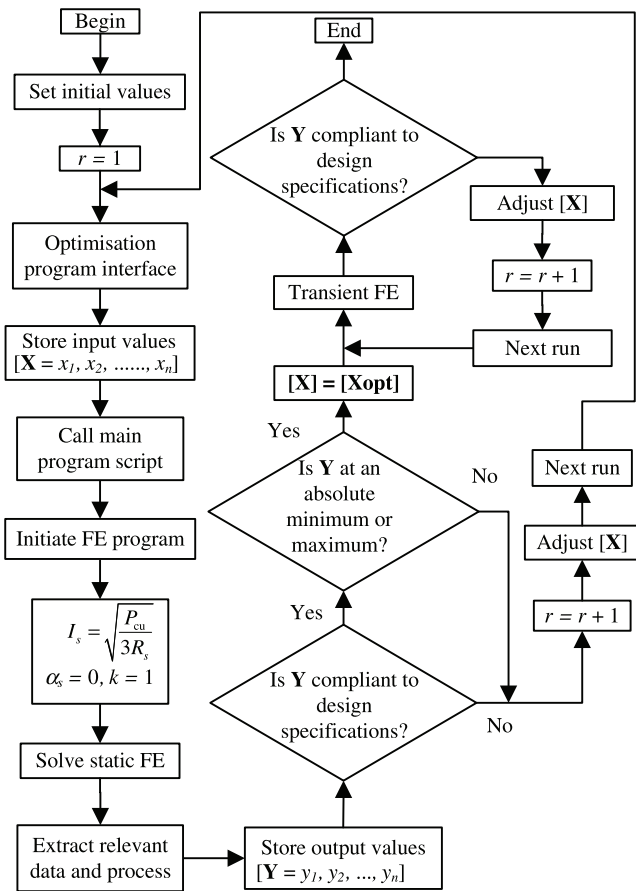


Fig. 5. Graphical representation of design optimization workflow.

by  $P_{wf}$  will be more or less similar for all of the different topologies.  $P_{ecs}$  can be estimated directly from FE-analysis with static simulations, but in order to calculate the PM losses in  $P_{ecr}$ , transient FE is required. As an estimation during the static FE design optimization,  $P_{ecr}$  is estimated as a percentage of  $P_{ecs}$ . After the initial static FE design optimization, these loss components are validated by means of transient FE-analysis. The mechanical loss ( $P_{wf}$ ) is calculated with the methods in [26].

#### IV. OPTIMIZATION RESULTS

Tables II and III give the optimization results versus turbine power rating for the nonoverlap- and conventional overlap-winding direct-drive PMSGs. Table IV gives the optimization results for the new concept toroidal-winding PMSG. Fig. 6 shows the active mass required per kW versus wind turbine power rating and Fig. 7 shows the PM mass per kW required. From Fig. 7, it can be seen that at the microwind power level ( $\leq 3$  kW), the toroidal-winding PMSG performs poor with regard to PM content compared to the other topologies. At this power level, the nonoverlap-winding performs the best. From about 15 kW, it is observed that the toroidal-winding generator performs much better. The reason for the poor performance of the toroidal-winding at the low-power levels is the increase in turbine speed and, thus, decrease in pole number

as given in Table I. Due to the increase in yoke heights with a decrease in pole count, the end-windings of the toroidal-winding become much longer, which decreases the generator's performance. Furthermore, with the outer diameter constraint, the inner PM rotor is also placed at a much less optimum airgap diameter.

From the upper medium scale to utility scale, it can be seen that the performance of the nonoverlap-winding generator decreases when compared to the other generator topologies, especially regarding PM content. At the utility scale, power level construction mass dominates the total mass as opposed to active mass. The PM content will, thus, have much more of an effect on the total cost. It is known that the power factor (PF) and kVA performance of the nonoverlap-winding machines are not as good as that of the conventional overlap-winding machines due to the much higher per-unit synchronous reactance ( $X_s$ ) of the nonoverlap-winding machines. This is also indicated in Tables III and IV by observing the much higher break down torque ( $T_b$ ) values achieved by the overlap and toroidal-winding machines due to the much lower  $X_s$  per-unit values of these machines. Furthermore, as shown in Fig. 4, the outer diameter gets much more constraint for the higher wind power levels with the torque requirement significantly higher. This makes torque generation even more challenging for the wind generators. The PF is shown in each case at the rated load value and the maximum torque per ampere operating point (rated  $q$ -axis current and zero  $d$ -axis current for surface-mount PM machines).

The nonoverlap-winding generator is shown to consistently comply the closest with the limits set for  $\Delta\tau_{NL}$  and  $\Delta\tau_L$ , with the conventional overlap-winding yielding the highest torque ripple in most cases. At lower power levels, it becomes increasingly more difficult for all of the topologies to adequately minimize the torque ripple. More elaborate torque ripple minimization techniques as described in [21], and also classical torque ripple reduction methods, e.g., skewing, can be employed in this case to reduce torque ripple. It is also shown in Table IV that it is possible to reduce the torque ripple of the toroidal-winding generator to within acceptable limits. For smaller generators, the possibility also exists to increase the number of slots per pole, which eases the reduction in the torque ripple as shown in Section V (Fig. 11).

Observing Fig. 8, which shows the ratio of the maximum allowable outer diameter to the generator axial stack length or aspect ratio, it is clear that the toroidal-winding has a much shorter axial length than the other topologies. Also shown in Tables II–IV is the torque developed per active stack volume ( $T_r/V_{act}$ ). At the utility scale, the toroidal-winding generator develops more than two times the torque per active stack volume! However, as shown in Table IV, the toroidal-winding generator does have a high loss per active volume. The thermal management of the toroidal-winding generator should, thus, be more thoroughly investigated in future studies. Some of the other parameters given in Tables II–IV include the generator inside diameter ( $D_i$ ), and the conductor and steel mass ( $M_{Cu}$  and  $M_{Fe}$ , respectively). At the medium- and utility-scale wind power levels, the toroidal-winding generator is shown to have the lowest total active mass.

TABLE II  
OPTIMIZATION RESULTS VERSUS TURBINE POWER OF THE NONOVERLAP DOUBLE LAYER PMSGs

	$T_b$ (pu)	$\Delta\tau_{NL}$ (%)	$\Delta\tau_L$ (%)	$P_{cu}$ (kW)	$P_{ecsr}$ (kW)	PF	$l$ (m)	$D_i$ (m)	$M_{PM}$ (kg)	$M_{Cu}$ (kg)	$M_{Fe}$ (kg)	$M_{Tot}$ (kg)	$P_{loss}/V_{act}$ (kW/m <sup>3</sup> )	$T_r/V_{act}$ (kNm/m <sup>3</sup> )	$J_s$ (A/mm <sup>2</sup> )
1 kW	2.62	4.46	11.90	0.037	0.037	0.960	0.0195	0.205	0.36	2.73	4.03	7.12	295.8	16.33	2.89
3 kW	2.45	4.56	10.39	0.100	0.097	0.968	0.037	0.416	1.21	6.09	13.39	20.69	354.7	39.53	3.63
15 kW	2.06	2.20	2.80	0.600	0.246	0.954	0.105	0.511	7.79	18.90	58.17	84.86	250.7	72.22	4.25
60 kW	1.25	3.38	3.39	2.820	0.451	0.924	0.174	1.063	24.04	84.48	166.3	274.8	387.0	173.48	4.26
300 kW	1.31	1.24	4.41	12.50	2.896	0.931	0.290	2.591	129.6	269.9	934.5	1334	137.53	391.44	4.96
1 MW	1.19	0.47	1.73	37.00	6.715	0.915	0.420	3.237	461.9	632.4	2642	3736	79.93	564.62	5.57
3 MW	1.46	0.97	2.06	115.0	13.169	0.935	1.300	4.770	1895	3018	8973	13885	59.79	832.49	4.48
7.5 MW	1.2	0.57	2.35	288.0	47.80	0.935	0.740	11.67	4951	3515	19778	28244	78.92	1348.09	6.14

TABLE III  
OPTIMIZATION RESULTS VERSUS TURBINE POWER OF THE CONVENTIONAL OVERLAP-WINDING PMSGs

	$T_b$ (pu)	$\Delta\tau_{NL}$ (%)	$\Delta\tau_L$ (%)	$P_{cu}$ (kW)	$P_{ecsr}$ (kW)	PF	$l$ (m)	$D_i$ (m)	$M_{PM}$ (kg)	$M_{Cu}$ (kg)	$M_{Fe}$ (kg)	$M_{Tot}$ (kg)	$P_{loss}/V_{act}$ (kW/m <sup>3</sup> )	$T_r/V_{act}$ (kNm/m <sup>3</sup> )	$J_s$ (A/mm <sup>2</sup> )
1 kW	4.25	19.26	39.97	0.037	0.035	1.000	0.028	0.1772	0.490	3.05	7.81	11.34	62.10	9.31	2.28
3 kW	2.03	8.85	18.34	0.170	0.054	0.926	0.045	0.3764	1.470	9.01	24.81	35.29	58.45	23.89	2.84
15 kW	3.11	13.37	31.52	0.684	0.218	0.991	0.1145	0.5232	7.820	25.22	60.77	93.91	66.84	71.61	3.40
60 kW	2.72	4.59	21.78	2.725	0.501	0.988	0.183	1.0728	29.54	76.02	162.1	267.7	82.51	176.89	3.91
300 kW	1.70	5.30	25.74	13.30	2.461	0.953	0.265	2.435	114.6	282.3	967.0	1364	99.37	396.98	4.58
1 MW	1.62	1.88	12.18	40.00	5.793	0.965	0.570	3.330	280.3	775.9	2117	3173	93.78	634.86	4.75
3 MW	1.68	2.23	15.40	121.3	13.49	0.964	1.400	4.774	1338	3122	10302	14762	59.26	786.38	4.10
7.5 MW	1.60	2.90	23.82	280.0	51.60	0.940	0.670	11.66	4120	3848	18427	26394	83.64	1445.75	5.57

TABLE IV  
OPTIMIZATION RESULTS VERSUS TURBINE POWER OF THE TOROIDAL-WINDING PMSGs

	$T_b$ (pu)	$\Delta\tau_{NL}$ (%)	$\Delta\tau_L$ (%)	$P_{cu}$ (kW)	$P_{ecsr}$ (kW)	PF	$l$ (m)	$D_i$ (m)	$M_{PM}$ (kg)	$M_{Cu}$ (kg)	$M_{Fe}$ (kg)	$M_{Tot}$ (kg)	$P_{loss}/V_{act}$ (kW/m <sup>3</sup> )	$T_r/V_{act}$ (kNm/m <sup>3</sup> )	$J_s$ (A/mm <sup>2</sup> )
1 kW	6.53	17.17	37.47	0.036	0.037	1.000	0.025	0.184	0.69	1.50	5.770	7.96	71.04	10.89	3.40
3 kW	3.32	12.36	23.18	0.167	0.068	1.000	0.026	0.357	1.94	6.92	12.44	21.31	90.55	36.92	3.30
15 kW	4.4	2.35	4.93	0.711	0.175	1.000	0.08	0.512	6.49	21.04	45.22	71.43	89.26	95.37	3.70
60 kW	1.66	0.45	4.50	2.712	0.866	0.999	0.095	0.964	26.51	97.4	177.98	301.9	99.14	192.89	3.99
300 kW	1.29	3.36	8.46	13.90	2.584	0.988	0.160	2.358	105.6	277.5	773.9	1157	257.26	986.01	4.68
1 MW	1.34	1.05	2.54	42.303	4.42	0.988	0.283	3.353	305.3	674.5	1986	2966	222.07	1473.8	5.24
3 MW	1.36	1.59	6.00	115.8	11.35	0.986	0.637	4.810	1292	2983	7888	12197	145.95	2047.6	4.08
7.5 MW	1.24	1.8	13.2	239.3	34.52	0.973	0.425	11.748	3588	3078	18909	25574	193.4	3063.69	6.71

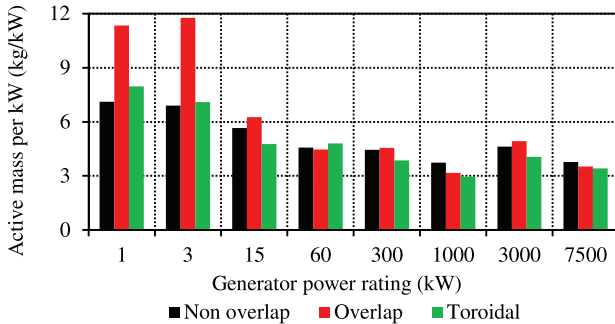


Fig. 6. Ratio of active mass per kW versus wind turbine power rating.

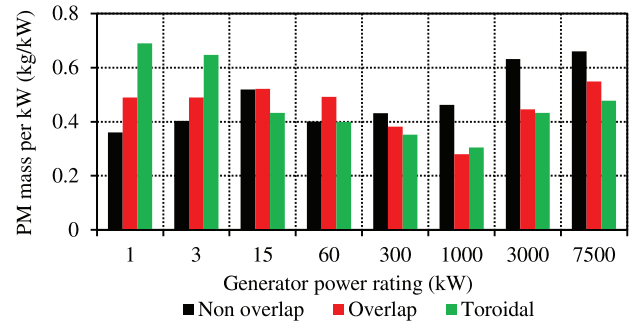


Fig. 7. Ratio of PM mass per kW versus wind turbine power rating.

## V. FURTHER TOROIDAL-WINDING ASPECTS

Although the main focus of this study is on the electromagnetic analysis of the toroidal-winding PMSG, several additional observations are made in the evaluation of this concept, as explained in this section.

### A. General Observations

Due to the manner in which the toroidal-winding stator is wound, it is possible to obtain a very good fill factor, and solid conductors can be used. However, in this case, eddy-current

losses in the conductors become a concern. It is well known that placing the conductors as in Fig. 9(a) will lead to very-high conductor eddy-current losses. For the toroidal-winding, though, the conductors are stacked as in Fig. 9(b), which is much more difficult to achieve with conventional winding layouts.

In the case of PM generators, to limit the PM losses, the PMs are usually segmented. However, as shown in Fig. 10, which indicates the PM rotor losses versus magnet segments,  $P_{ecr}$  for the toroidal-winding PMSG is very low, even if solid magnets are employed. The nonoverlap-winding generator, on the other hand, has much higher PM losses even when segmented.

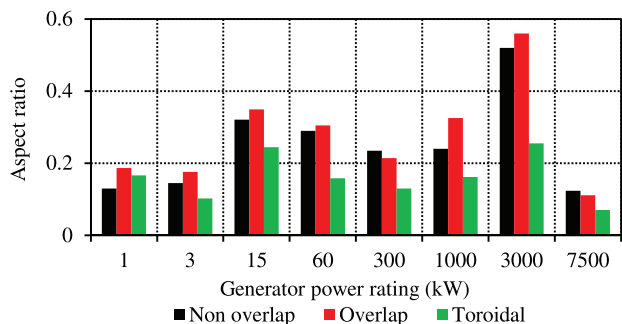


Fig. 8. Ratio of generator outer diameter to axial stack length versus wind turbine power rating.

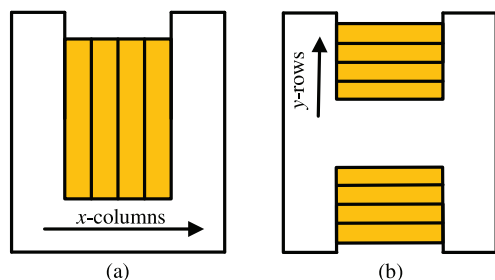


Fig. 9. Conductors segmented in (a) horizontal ( $x$ ) direction and (b) vertical ( $y$ ) direction.

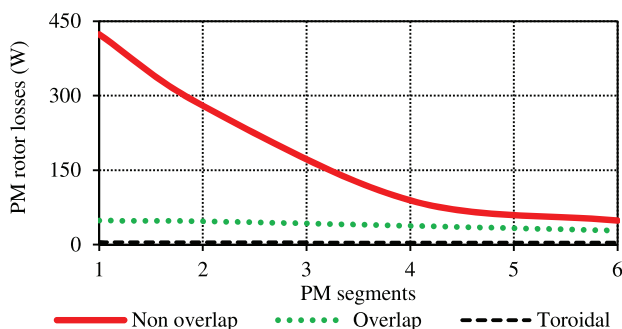


Fig. 10. FE-calculated PM rotor loss versus PM segments for the optimum designed nonoverlap, conventional overlap, and prototype toroidal-winding PMSGs.

Thus, solid magnets and solid rotor back yokes can easily be utilized for the toroidal-winding PMSG without any additional losses. Due to the way the toroidal-winding is wound, it is easier to accommodate more stator slots as opposed to conventional overlap-windings, which is why it has a lower PM-rotor loss than the conventional overlap-winding generator.

Fig. 11 shows the magnitude of  $\Delta\tau_{NL}$  versus the number of slots per pole. It is clear that  $\Delta\tau_{NL}$  decreases with an increase in the number of slots per pole. With the use of two PM rotors, the two rotors can also be offset from one another to reduce the combined torque ripple magnitude as shown in the next section (Fig. 14).

### B. Summary of Advantages and Disadvantages

The main preliminary advantages and disadvantages of the toroidal-winding PMSG can be summarized as below. It should,

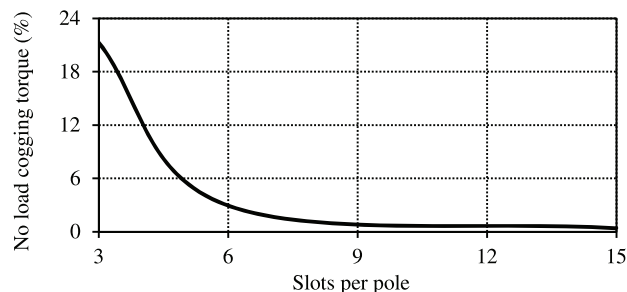


Fig. 11. FE-calculated no-load cogging torque of the optimum 15-kW toroidal-winding PMSG versus number of slots per pole.

however, be noted that many aspects of the toroidal-winding PMSG still require further investigation:

- 1) shorter end-windings than conventional overlap-windings;
- 2) easy stator stack segmentation due to no coils overlapping;
- 3) much better torque performance compared to nonoverlap-winding PMSGs;
- 4) higher fill factors can be achieved more easily. Practically, fill factors of up to 0.7 were easily obtained with test winding pieces;
- 5) placement of conductors allows for easier mitigation of conductor eddy-current losses;
- 6) low PM rotor losses, which means that solid yokes and PMs can be considered;
- 7) better torque ripple characteristics compared to conventional overlap-winding topologies;
- 8) shorter stack length and, thus, higher torque density;
- 9) although more comment is required from industry, the windings seem relatively easy to manufacture;
- 10) not suited for high-speed applications with low pole numbers, due to the increase in common stator yoke height and more flux coupling between the two PM rotors;
- 11) manufacturing, especially regarding the placement and fixing of the stator segments, is the biggest question. There are methods available to fix these segments together by utilizing holes in the common stator yoke similarly as used for the prototype generator discussed in the next section. Careful attention should be given to any unbalanced radial attraction forces;
- 12) as shown, the toroidal-winding generator does have a high loss per unit volume. Heat dissipation might, thus, be a problem for high current density applications. However, the two PM rotor configuration might help to improve the airflow and convection, but further analysis is required.

## VI. PERFORMANCE EVALUATION

For the experimental generator performance evaluation, only the toroidal-winding PMSG is evaluated. The performance of the nonoverlap-winding PMSG is evaluated more thoroughly in [16]. The manufacturing and practical evaluation of a conventional overlap-winding PMSG is not considered, as this type of machine has been evaluated in numerous other studies in literature.

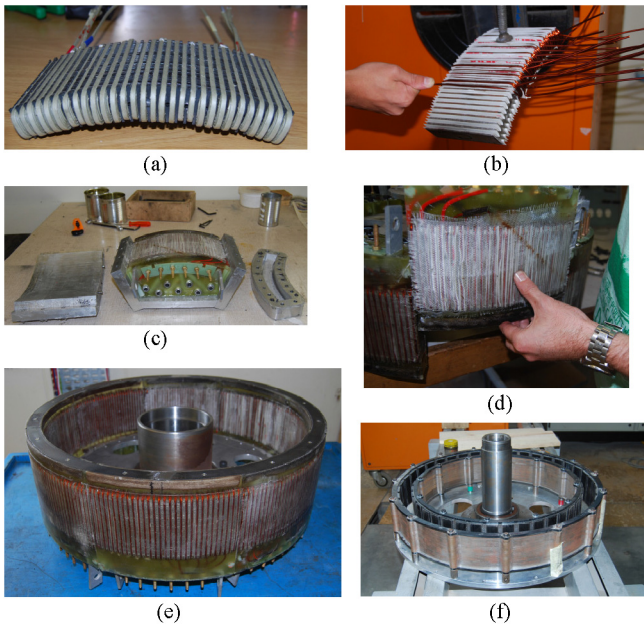


Fig. 12. (a) Manufactured toroidal test winding section with rectangular wire. (b) Toroidal-winding section being wound. (c) Winding section in mould. (d) Moulded winding section being shifted into position. (e) Completed toroidal-winding stator. (f) Double PM rotor.

### A. Prototype Generator

The prototype (15 kW, 1 kNm) toroidal-winding PMSG is manufactured by modifying the double rotor, nonoverlap-winding PMSG of [12] shown in Fig. 2(b). Due to the modification of an existing machine structure, it should be noted that the prototype toroidal-winding machine is not an optimum design; the resulting machine is merely a quick modification to verify the operational principles of this machine type. As in [12], the stator is divided into eight sections and is manufactured by moulding each stator section in epoxy resin. As shown in the field plot of Fig. 3(c) in Section II, holes are made in the center of the common stator yoke through which stainless steel rods are inserted. These stainless steel rods together with two stainless steel clamps are used to hold the laminations of each section together. The moulded stator sections are fixed to a stator mounting plate and inserted between the two PM-rotors. It must be mentioned that stator assembling and support can also be implemented without using epoxy. Fig. 12(a) shows an experimental toroidal-winding stator section making use of rectangular wire and Fig. 12(b) shows the toroidal-winding stator section being wound. Fig. 12(c) shows a toroidal-winding stator section inside the mould and (d) shows a stator section being shifted into position. Fig. 12(e) and (f) shows the completed toroidal-winding stator and PM rotor, respectively. The prototype generator on the test bench in the laboratory is shown in Fig. 13.

### B. Performance Results

Fig. 14 shows the FE-predicted no-load cogging torque, and load torque ripple at rated load. The no-load torque developed by both inner and outer PM rotor parts are shown in Fig. 14.



Fig. 13. Prototype toroidal-winding PMSG mounted on the test bench in the laboratory.

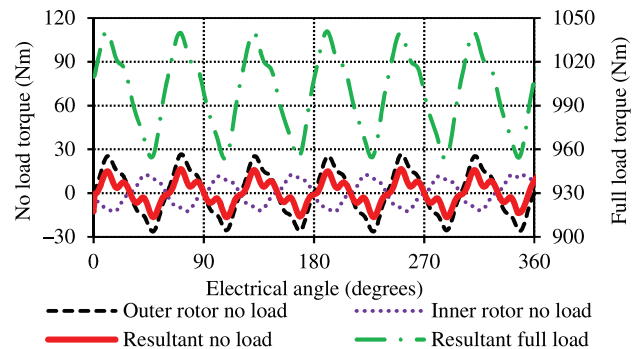


Fig. 14. FE-predicted no-load cogging torque and load torque ripple of the 15-kW toroidal-winding PMSG prototype.

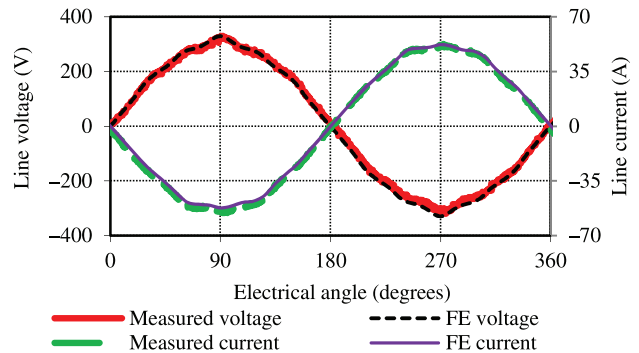


Fig. 15. FE-predicted and measured open-circuit line voltage and line current at rated load versus electrical angle of the toroidal-winding PMSG.

During manufacturing, the PMs of the two PM rotor parts can be offset by a skewing angle corresponding to one slot pitch. As seen in Fig. 14, the torque ripple is not completely removed. This is because the experimental machine not being optimized for low-torque ripple with the torque ripple waveforms of the outer and inner PM rotor parts having different harmonic components.

Fig. 15 shows the open-circuit induced voltage waveform and the line current at rated load of the toroidal-winding PMSG. In order to give an indication on the torque performance of the toroidal-winding PMSG Fig. 16 shows the short-circuit torque versus speed performance (measured up to more than 2.0 p.u. torque) of the prototype toroidal-winding, nonoverlap double layer PMSG as evaluated in [16], and the double rotor nonoverlap-winding PMSG as evaluated in [12]. Clearly, the toroidal-winding PMSG is shown to achieve a much higher maximum torque due to its relatively low synchronous reactance. The mechanical input power and electrical output power,

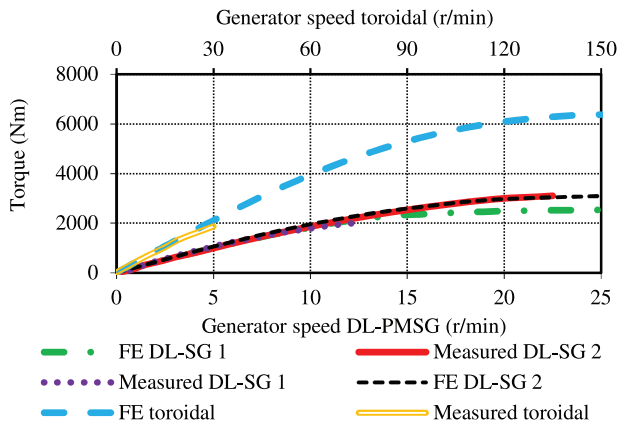


Fig. 16. FE-predicted and measured braking (short-circuit) torque profiles of the nonoverlap PMSGs of Fig. 2(a) (DL-SG 1) and Fig. 2(b) (DL-SG 2) and the toroidal-winding PMSG of Fig. 2(c) versus generator speed.

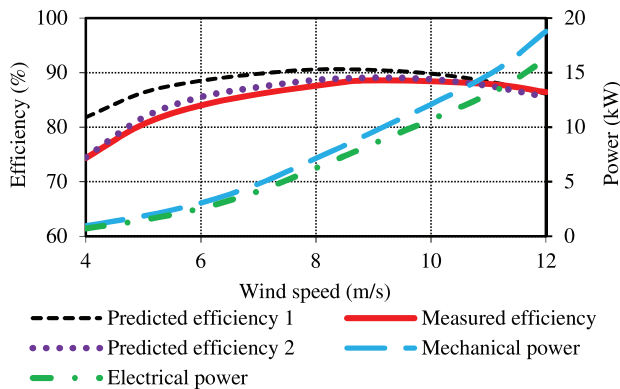


Fig. 17. Measured and predicted efficiency [including two different values for  $P_{wf}$  (Prediction 1 use calculated mechanical loss and Prediction 2 use measured mechanical loss values)], as well as the measured mechanical input and electrical output power versus wind speed ( $v_{w(\min)} = 4$  m/s and  $v_{w(\text{rated})} = 11$  m/s) at the turbine maximum power point tracking values of the toroidal-winding PMSG.

as well as the measured and FE-predicted efficiencies of the toroidal-winding PMSG as a function of maximum turbine-power-points are shown in Fig. 17. At a wind speed of  $v_w = 11$  m/s,  $n_s = 150$  r/min, the generator is at rated conditions, i.e., 15 kW at 1000 Nm and 88% efficiency. The reason for the difference between the measured and the FE-predicted efficiencies is discussed in the next section.

### C. Mechanical Loss Investigation

The difference between the predicted loss and the measured loss is much more observable at low loads, which indicates that the no-load losses are incorrectly predicted. Due to the importance of this loss component in the partially rated region for wind turbines, where they tend to operate most of the time, it is important that the no load losses are estimated correctly. Furthermore, it is necessary that these losses are better understood if they are to be minimized during design optimization.

The no-load losses consists of four components with

$$P_{NL} = P_{ecs} + P_{ecr} + P_{wf} + P_{cuc} \quad (3)$$



Fig. 18. (a) Dummy stator mould being prepared with plastic pellets and epoxy resin and (b) completed nonmagnetic dummy stator section.

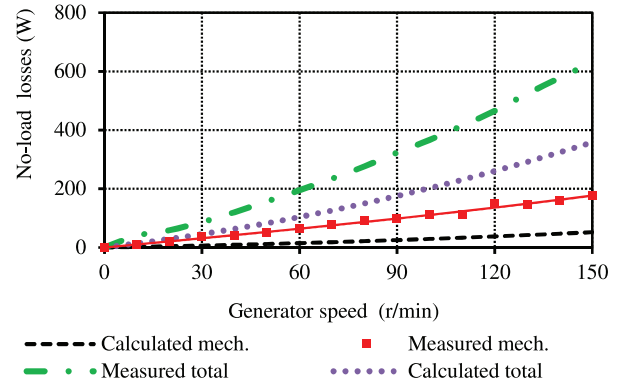


Fig. 19. Predicted and measured mechanical loss and total no load loss versus generator speed of the toroidal-winding PMSG.

If solid conductors are used, the ac conductor losses ( $P_{cuc}$ ) should also be taken into account. For the toroidal-winding generator,  $P_{ecr}$  is expected to be almost negligible as shown in Fig. 10, especially since the experimental machine utilizes segmented magnets. Although the accurate calculation of  $P_{ecs}$  depends on the use of the correct core loss coefficients, the steel type used is quite commonly used throughout the industry, which means that the prediction of this loss component should be quite accurate.  $P_{cuc}$  should also be fairly low due to the low electrical frequency ( $f_s = 50$  Hz). A good prediction of this loss component is also obtained from FE. Thus, the loss component most susceptible to calculation errors is the mechanical loss.

Due to the use of PMs and to accurately take into account the windage losses, a nonmagnetic “dummy” stator is manufactured. Fig. 18 shows the manufacturing of a stator section with nonmagnetic materials. The stator of Fig. 12(e) is replaced with this nonmagnetic stator.

Fig. 19 shows the loss calculated by means of the methods in [26] versus the measured result as well as the total predicted and measured no-load losses. Clearly, there is a large difference between the calculated and the measured mechanical loss component. Fig. 17 shows how this incorrect loss calculation affects the efficiency calculation. Hence, the partial load efficiency is predicted much more accurate by including the measured mechanical losses.

It is possible that the mechanical losses were predicted incorrectly in this case due to bearing misalignment or damage during assembly. However, the same tendency was observed for the same size nonoverlap-winding wind generators evaluated in [21] and [16], where the no-load losses were significantly

underestimated. From this mechanical loss evaluation, the importance of correctly estimating this loss component is clear, which is an aspect that should be more adequately investigated in future studies.

## VII. CONCLUSION

In this paper, the toroidal-winding PMSG is shown to perform well regarding active mass and especially PM content for a wide range of wind turbine powers. Only at the small- and micropower levels, the toroidal-winding PMSG is shown not to be a suitable option, with this machine type not suited for low pole number applications. It performs better than conventional overlap-winding PMSGs due to the shorter end-windings of this generator. At the small- and micropower levels, the nonoverlap-winding PMSG should be the most suitable option. Even at the lower medium scale, this generator could still be an option due to its favorable characteristics regarding torque ripple and ease of manufacturing. However, at the utility-scale level, the amount of PM material required by the nonoverlap-winding increases significantly as compared to the other generator topologies.

Although the performance of the toroidal-winding PMSG is throughout to some extent better than that of the overlap-winding PMSG at the utility-scale power level, there are also several other favorable characteristics of the toroidal-winding PMSG to consider. These are, e.g., higher torque density, easier reduction in torque ripple, easier segmentation, and reduced conductor eddy currents and PM losses. There are, however, several aspects of the toroidal-winding PMSG which need to be investigated further, such as structural and thermal analysis as well as some further study on the manufacturing processes. In this study, the focus was merely to provide an electromagnetic analysis regarding the applicability of the toroidal-winding PMSG over the whole wind turbine power range. With the electromagnetic characteristics known and the operating principles of the toroidal-winding PMSG validated by means of the manufactured prototype, future studies can now focus more on the implementation of this generator type.

It is also shown in this study that the mechanical loss component of direct-drive wind generators can easily be underestimated. This aspect should be addressed in future studies as it could significantly influence the partial load performance of wind generators. Another aspect is the higher loss density found for the toroidal-winding PMSG, which can cause thermal issues and which must be investigated. In terms of cooling, it must be mentioned that the toroidal PMSG has two air gaps through which cooling can take place; it has, thus, a double-sided cooled stator. Finally, the toroidal-winding generator might also be quite well suited for double rotor axial-flux motors, as in this case both rotors are placed at an optimum torque diameter.

## REFERENCES

- [1] H. Polinder, J. A. Ferreira, B. B. Jensen, A. B. Abrahamsen, K. Atallah, and R. A. McMahon, "Trends in wind turbine generator systems," *IEEE J. Emerging Sel. Topics Power Electron.*, vol. 1, no. 3, pp. 174–185, Sep. 2013.
- [2] H. Li, Z. Chen, and H. Polinder, "Optimization of multibrid permanent-magnet wind generator systems," *IEEE Trans. Energy Convers.*, vol. 24, no. 1, pp. 82–92, Mar. 2009.
- [3] H. Polinder, F. F. A. van der Pijl, G. J. de Vilder, and P. Tavner, "Comparison of direct-drive and geared generator concepts for wind turbines," *IEEE Trans. Energy Convers.*, vol. 21, no. 3, pp. 725–733, Sep. 2006.
- [4] D. Bang, H. Polinder, G. Shrestha, and J. A. Ferreira, "Review of generator systems for direct-drive wind turbines," in *Proc. Eur. Wind Energy Conf. (EWEC)*, Brussels, Belgium, 2008, pp. 1–11.
- [5] D. Bang, H. Polinder, G. Shrestha, and J. A. Ferreira, "Promising direct-drive generator system for large wind turbines," in *Proc. Wind Power Grid-EPE Wind Energy Chapter 1st Seminar (EPE-WECS)*, Delft, Netherlands, 2008, pp. 1–10.
- [6] H. Li and Z. Chen, "Overview of different wind generator systems and their comparisons," *IET Renew. Power Gener.*, vol. 2, no. 2, pp. 123–138, Jun. 2008.
- [7] M. A. Mueller and A. S. McDonald, "A lightweight low-speed permanent magnet electrical generator for direct-drive wind turbines," *Wind Energy*, vol. 12, no. 8, pp. 768–780, 2009.
- [8] R. Scott Semken *et al.*, "Direct-drive permanent magnet generators for high power wind turbines: Benefits and limiting factors," *IET Renew. Power Gener.*, vol. 6, no. 1, pp. 1–8, Jan. 2012.
- [9] J. N. Stander, G. Venter, and M. J. Kamper, "Review of direct drive radial flux wind turbine generator mechanical design," *Wind Energy*, vol. 15, no. 3, pp. 459–472, 2012.
- [10] Z. Zhanga, A. Chen, A. Matveev, R. Nilssen, and A. Nysveena, "High-power generators for offshore wind turbines," *Energy Proc.*, vol. 35, no. 2013, pp. 52–61, 2013.
- [11] A. H. Isfahani, A. H. Boroujerdi, and S. Hasanzadeh, "Multi-objective design optimization of a large-scale direct drive permanent magnet generator for wind energy conversion systems," *Front. Energy*, vol. 8, no. 2, pp. 182–191, 2014.
- [12] J. H. van Wijk and M. J. Kamper, "Double-sided rotor technology for iron-cored permanent magnet wind generators: An evaluation," in *Proc. IEEE Int. Conf. Ind. Technol. (ICIT'13)*, Cape Town, South Africa, 2013, pp. 1892–1897.
- [13] R. Qu and T. Lipo, "Dual-rotor, radial-flux, toroidally wound permanent-magnet machines," *IEEE Trans. Ind. Appl.*, vol. 39, no. 6, pp. 1665–1673, Nov./Dec. 2003.
- [14] Y. Yeh, M. Hsieh, and D. Dorell, "Different arrangements for dual-rotor dual-output radial-flux motors," *IEEE Trans. Ind. Appl.*, vol. 48, no. 2, pp. 612–622, Mar./Apr. 2012.
- [15] P. Xu, X. Liu, K. Shi, and Y. Du, "Design of dual-rotor radial flux permanent-magnet generator for wind power applications," *Appl. Mech. Mater.*, vols. 416–417, pp. 9–14, 2013.
- [16] J. H. J. Potgieter and M. J. Kamper, "Design optimization of directly grid-connected PM machines for wind energy applications," *IEEE Trans. Ind. Appl.*, vol. 51, no. 4, pp. 2949–2958, Jul./Aug. 2015.
- [17] A. Grauers, "Design of direct-driven permanent-magnet generators for wind turbines," Ph.D. dissertation, Dept. Elect. Power Eng., Elect. Mach. Power Electron., Chalmers Univ. Technol., Göteborg, Sweden, 1996.
- [18] G. Shrestha, H. Polinder, and J. A. Ferreira, "Scaling laws for direct drive generators in wind turbines," in *Proc. IEEE Int. Conf. Elect. Mach. Drives (IEMDC)*, Miami, FL, USA, 2009, pp. 797–803.
- [19] A. Huskey and D. Prascher, "Tower design load verification on a 1-kW wind turbine," in *Proc. 43rd AIAA Aerosp. Sci. Meeting Exhibit*, Reno, NV, USA, 2005, pp. 1–7.
- [20] J. A. Stegmann and M. J. Kamper, "Design aspects of double-sided rotor radial flux air-cored permanent-magnet wind generator," *IEEE Trans. Ind. Appl.*, vol. 47, no. 2, pp. 767–778, Mar./Apr. 2011.
- [21] J. H. J. Potgieter and M. J. Kamper, "Torque and voltage quality in design optimization of low cost non-overlap single layer winding permanent magnet wind generator," *IEEE Trans. Ind. Electron.*, vol. 59, no. 5, pp. 2147–2156, May 2012.
- [22] M. J. Kamper, "Development and test results of South Africa's first 300 kW permanent magnet direct drive grid connected wind generator system," presented at the 18th Southern African Univ. Power Eng. Conf. (SAUPEC), Stellenbosch, South Africa, 2009.
- [23] Enercon. (2015, Sep. 13). *Enercon E-126 / 7 580 kW* [Online]. Available: <http://www.enercon.de/en-en/66.htm>.
- [24] Windpower Monthly. (2015, Sep. 13). *Close Up—The E126, Still the World's Biggest Turbine* [Online]. Available: <http://www.windpowermonthly.com/article/1138562/close—e126-worlds-biggest-turbine>.
- [25] J. Sapanen, V. Ruuskanen, J. Nerg, and J. Pyrhönen, "Dynamic torque analysis of a wind turbine drive train including a direct-driven permanent magnet generator," *IEEE Trans. Ind. Electron.*, vol. 58, no. 9, pp. 3859–3867, Sep. 2011.
- [26] J. Pyrhönen, T. Jokinen, and V. Hrabovcová, *Design of Rotating Electrical Machines*, 1st ed. Hoboken, NJ, USA: Wiley, 2008.

- [27] Y. Alexandrova, S. Semken, M. Polikarpova, and J. Pyrhönen, "Defining proper initial geometry of an 8 MW liquid-cooled direct-drive permanent magnet synchronous generator for wind turbine applications based on minimizing mass," in *Proc. 20th IEEE Int. Conf. Elect. Mach. (ICEM)*, Marseille, France, 2012, pp. 1250–1255.
- [28] H. Polinder, D. Bang, R. P. J. O. M. van Rooij, A. S. McDonald, and M. A. Mueller, "10 MW wind turbine direct-drive generator design with pitch or active speed stall control," in *Proc. IEEE Int. Conf. Elect. Mach. Drives (IEMDC)*, Antalya, Turkey, 2007, pp. 1390–1395.
- [29] *VisualDOC Users Manual*, version 6, Vanderplaats Research & Development, Inc., Colorado Springs, CO, USA, 2006.
- [30] Y. Duan and D. M. Ionel, "A review of recent developments in electrical machine design optimization methods with a permanent-magnet synchronous motor benchmark study," *IEEE Trans. Ind. Appl.*, vol. 49, no. 3, pp. 1268–1275, May/Jun. 2013.



**Johannes H. J. Potgieter** (M'15) received the B.Eng. degree in electrical and electronic engineering and the M.Sc. (Eng.) and Ph.D. (Eng.) degrees in electrical engineering from the University of Stellenbosch, Stellenbosch, South Africa, in 2008, 2011, and 2014, respectively.

Since May 2014, he has been a Postdoctoral Research Assistant with the University of Oxford, Oxford, U.K. His research interests include wind power generation technologies, hybrid-electrical automotive drive train solutions, and the design and optimization of permanent-magnet and switched reluctance electrical machines.



**Maarten J. Kamper** (SM'08) received the M.Sc. and Ph.D. degrees in engineering from the University of Stellenbosch, Stellenbosch, South Africa, in 1987 and 1996, respectively.

Since 1989, he has been with the Academic Staff of the Department of Electrical and Electronic Engineering, University of Stellenbosch, where he is currently a Professor of Electrical Machines and Drives. His research interests include computer-aided design and control of reluctance, permanent-magnet, and induction machine drives.

Dr. Kamper is a South African National Research Foundation Supported Scientist and a Registered Professional Engineer in South Africa.